

## Time-resolved Fluorescence Spectra of Arterial Fluorescent Compounds: Reconstruction with the Laguerre Expansion Technique

Jean-Michel I. Maarek<sup>\*1</sup>, Laura Marcu<sup>1,2</sup>, Wendy J. Snyder<sup>1,2</sup> and Warren S. Grundfest<sup>2</sup>

<sup>1</sup>Department of Biomedical Engineering, University of Southern California, Los Angeles, CA, USA and

<sup>2</sup>Laser Research & Technology Development Laboratory, Cedars Sinai Medical Center, Los Angeles, CA, USA

Received 5 July 1999; accepted 1 November 1999

### ABSTRACT

The time-resolved fluorescence spectra of the main arterial fluorescent compounds were retrieved using a new algorithm based on the Laguerre expansion of kernels technique. Samples of elastin, collagen and cholesterol were excited with a pulsed nitrogen laser and the emission was measured at 29 discrete wavelengths between 370 and 510 nm. The expansion of the fluorescence impulse response function on the Laguerre basis of functions was optimized to reproduce the observed fluorescence emission. Collagen lifetime (5.3 ns at 390 nm) was substantially larger than that of elastin (2.3 ns) and cholesterol (1.3 ns). Two decay components were identified in the emission decay of the compounds. For collagen, the decay components were markedly wavelength dependent and hydration dependent such that the emission decay became shorter at higher emission wavelengths and with hydration. The decay characteristics of elastin and cholesterol were relatively unchanged with wavelength and with hydration. The observed variations in the time-resolved spectra of elastin, collagen and cholesterol were consistent with the existence of several fluorophores with different emission characteristics. Because the compounds are present in different proportions in healthy and atherosclerotic arterial walls, characteristic differences in their time-resolved emission spectra could be exploited to assess optically the severity of atherosclerotic lesions.

### INTRODUCTION

Laser-induced fluorescence spectroscopy has been widely investigated as a nondestructive optical technology for medical diagnostics. In particular, application to the detection and characterization of atherosclerotic lesions has been studied *in vitro* (1–4) and *in situ* (5). Differences in the continuous

wave (CW)<sup>†</sup> fluorescence spectra of healthy and atherosclerotic arterial tissue were interpreted in terms of wall composition (2–4). The structural protein elastin was the most important contributor to the fluorescence of healthy arterial wall (2,3). Collagen on the surface of advanced plaque lesions was responsible for the emission of atherosclerotic arterial walls (4). Lipids, including free cholesterol, that invade plaque lesions during the atherosclerotic process have also been shown to fluoresce under intense UV laser excitation (2,4,6).

Selective absorption of the fluorescence emission by blood hemoglobin and other endogenous chromophores complicates the interpretation of arterial spectra in terms of wall composition (3). A few studies (7–10) suggested that lifetime information that is not affected by selective absorption could be used to increase the diagnostic capability of fluorescence spectroscopy. The fluorescence emission of atherosclerotic plaques lasted longer than the emission of healthy vessel walls (7–9), which was interpreted in terms of the longer lasting emission of collagen compared to elastin (10). The time-resolved emission of arterial fluorescent compounds was only measured at one or two wavelengths in these studies. Wavelength-dependent variations of the time-dependent decay would add a new dimension of information to the spectral data that could be exploited to better identify atherosclerotic lesions and to assess more precisely tissue composition. To our knowledge, the time-resolved emission spectra of fluorescent compounds of the arterial wall have been investigated only in a limited way (10,11).

To estimate the intrinsic fluorescence decay of a compound, the observed fluorescence trace must be deconvolved from the excitation pulse (12,13). The most commonly used deconvolution technique is the least-squares iterative reconstruction (LSIR) technique (12,14,15). This technique applies a least-squares minimization algorithm to compute the coefficients of a multiexponential expansion of the fluorescence decay. For complex fluorescent compounds like elastin and collagen, the multiexponential expansion is often a best-fit solution to the numerical deconvolution problem. Its coefficients are not readily interpretable in terms of fluoro-

<sup>\*</sup>To whom correspondence should be addressed at: Department of Biomedical Engineering, University of Southern California, Los Angeles, CA 90089-1451, USA. Fax: 213-740-0343; e-mail: jmaarek@bmsrs.usc.edu

© 2000 American Society for Photobiology 0031-8655/00 \$5.00+0.00

<sup>†</sup>Abbreviations: CW, continuous wave; HWHM, half width at half maximum; FWHM, full width at half maximum; IRF, impulse response function; LSIR, least-squares iterative reconstruction; NA, numerical aperture.

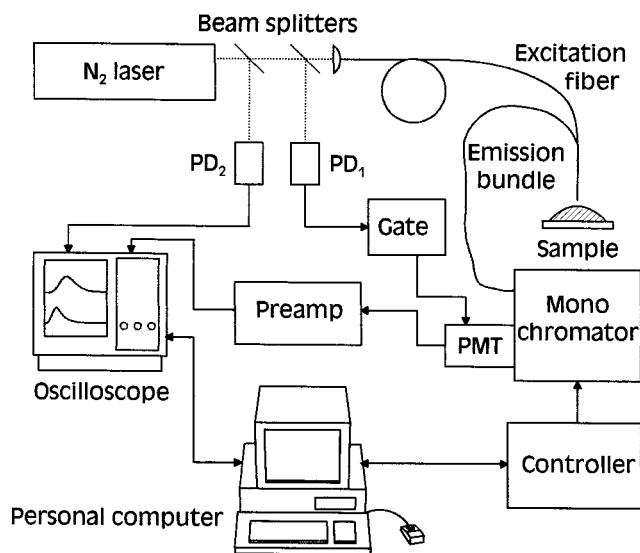


**Figure 1.** Spectroscopy setup used to measure the time-resolved fluorescence spectra of arterial fluorescent compounds. PD<sub>1</sub> and PD<sub>2</sub>, photodetectors; PMT, multichannel plate photomultiplier tube; Pre-amp, 1 GHz preamplifier; Gate, gate-and-delay generator.

phore response (13,16). Marmarelis (17) proposed to use an expansion on the discrete time Laguerre basis to deconvolve the intrinsic properties of a dynamic system from experimental input–output data. Because the Laguerre basis is a complete family of functions, a unique and desirable characteristic of this approach is that it can reconstruct a fluorescence response of arbitrary form. The latter could then be tested against different possible models to characterize the photophysical processes responsible for the emission (16).

Therefore, this study had two goals. First, we investigated the applicability of the Laguerre expansion technique for deconvolution of the time-resolved decay of arterial fluorescent compounds. Second, we characterized the time-resolved emission spectra of arterial fluorescent compounds to determine if knowledge of the time-resolved spectra would improve the diagnostic power of arterial fluorescence spectroscopy.

## MATERIALS AND METHODS

**Excitation delivery and fluorescence detection.** In the experimental setup (Fig. 1), the output pulse of a free-running nitrogen laser (EG&G, model 2100;  $\lambda$ : 337 nm; pulse width: 3 ns full width at half maximum [FWHM]; pulse repetition rate: 10 Hz) was focused on the extremity of a UV-grade silica fiber (core diameter: 600  $\mu\text{m}$ ; numerical aperture [NA] = 0.22) that directed the laser emission to the sample from above (spot size:  $\sim 1.8 \text{ mm}^2$ ). Six silica optic fibers (600  $\mu\text{m}$ ; NA = 0.22) positioned around the excitation fiber collected and guided the fluorescence emitted by the sample to the input slit of a scanning 1/4 m monochromator (Oriel, 77200; F/4.4; UV-visible grating, model 77232; 1200 grooves/mm; bandpass: 5 nm FWHM). A gated microchannel plate photomultiplier tube (Hamamatsu, R2024U; rise time: 0.3 ns; high voltage: 1800–2200 V) placed against the exit slit detected the fluorescence emission at the wavelength selected on the monochromator. The photomultiplier output was amplified with a fast alternating current preamplifier (EG&G Ortec, 9306; rise time: 0.35 ns; bandwidth: 100 kHz to 1 GHz; gain: 100) and digitized with a digital oscilloscope (Tektronix, TDS640; bandwidth: 500 MHz; sampling frequency: 2 Gsamples/s).

A longpass filter (345 nm) at the exit of the monochromator prevented most of the laser light reflected by the sample from reaching

the photomultiplier. With the monochromator tuned to near the laser line, the amount of reflected laser light that passed through the filter was sufficient for measuring the laser pulse waveform.

A fraction of the laser output was diverted with two beam splitters toward two fast silicon photodetectors. One detector (Newport, 818-BB-21) connected to a gate-and-delay generator (EG&G Ortec, model 416 A) gated the photomultiplier (gate duration: 5  $\mu\text{s}$ ). The other photodetector (EG&G Parc, model 2100/99) triggered the oscilloscope and monitored the pulse-to-pulse fluctuations of the laser output energy.

The experimental setup was automated with a personal computer (AST Research) interfaced (GPIB) with the oscilloscope and the stepper motor controller in the monochromator wavelength drive (Oriel, 77228). The computer program controlled the displacement of the monochromator grating and the transfer of the waveforms sampled by the oscilloscope (fluorescence and laser pulses) to permanent storage on the computer hard drive.

**Samples.** Time-resolved spectra were obtained from commercially purified samples of primary sources of fluorescence in healthy arterial wall and atherosclerotic plaque: elastin, type I collagen and cholesterol. Samples of bovine neck ligament elastin, type I insoluble Achilles tendon collagen and cholesterol (Sigma Chemical) were studied at room temperature in a nonfluorescent cell open to the atmosphere. Because the compounds are normally found in the watery tissue environment, which could alter their fluorescence response (18,19), they were studied both dry and hydrated with 0.9% NaCl solution. Hydrated samples were prepared by thoroughly mixing the sample material with saline and allowing the saline to permeate the material for at least 5 min.

**Experimental procedures.** The fluorescence response was measured at 29 wavelengths ranging from 370 to 510 nm (5 nm increment) selected to capture the whole spectral emission of compounds when excited in the UV (2,4). To improve the signal-to-noise ratio, each recorded fluorescence transient consisted on average of 16 consecutive fluorescence pulses computed by the oscilloscope circuitry before transfer to the personal computer. After receiving data from the oscilloscope, the computer shifted the monochromator output wavelength by 5 nm and reset the oscilloscope for the next fluorescence measurement. The voltage sensitivity of the oscilloscope was periodically readjusted as the fluorescence intensity changed with wavelength to optimize the choice of voltage resolution for the digital-to-analog converter in the oscilloscope's vertical system. Ten consecutive measurements of the fluorescence response were collected for three wavelengths (390, 430, 470 nm) to assess the variability of the fluorescence measurement across the emission spectrum. For each compound, fluorescence measurements were obtained on three different samples of the same lot.

The energy output of the laser was adjusted to 0.6  $\mu\text{J}/\text{pulse}$ . Under the experimental conditions of the study, the total fluence delivered to the illuminated site at the end of a measurement sequence lasting 370 s, *i.e.* the total energy delivered per unit area, was  $< 1.2 \text{ mJ}/\text{mm}^2$ . Under such conditions, photobleaching of the sample emission was expected to induce only minor alterations of the fluorescence spectra (6).

After the fluorescence measurements were completed, the monochromator was adjusted to a wavelength slightly below the laser line. The exact wavelength was selected such that the detected amplitude of the laser pulse reflected by the sample was in the range of the largest amplitude observed during the fluorescence measurements. Sixteen laser pulses reflected by the sample were averaged and used to represent the shape of the excitation pulse. The same vertical sensitivity was used for measurement of the laser pulse and the fluorescence response at the peak of emission, which resulted in identical voltage resolutions for the laser and fluorescence waveforms. Background noise was measured with the monochromator tuned to 400 nm after removing the sample and lifting the excitation-collection fiber assembly away from the optical bench. The background noise was subtracted from the laser input and fluorescence response signals.

**Deconvolution method.** The LSIR technique (12) has been retained as the most effective approach for deconvolution of the emission decay measured in time-resolved fluorescence spectroscopy (13–15). We experimented with a variant of LSIR in which the fluorescence impulse response function (IRF) was expressed as an

expansion on the discrete time Laguerre basis (17,20) instead of a weighted sum of exponential functions.

The relationship between the fluorescence response  $y(n)$  ( $n = 0 \dots N - 1$ ) and the laser pulse  $x(n)$  is expressed by the convolution equation:

$$y(n) = T \cdot \sum_{m=0}^{M-1} h(m)x(n - m) \quad (1)$$

where  $h(m)$  represents the fluorescence IRF ( $m = 0 \dots M - 1$ ) and  $T$  is the sampling period. To retrieve the fluorescence IRF, we considered the expansion of  $h(m)$  on the orthonormal basis of discrete-time Laguerre functions  $\{L_i(\alpha, m)\}$ :

$$h(m) = \sum_{i=0}^I c_i L_i(\alpha, m) \quad (2)$$

with

$$L_i(\alpha, m) = \alpha^{(m-i)/2} (1 - \alpha)^{1/2} \sum_{k=0}^i (-1)^k \binom{m}{k} \binom{i}{k} \alpha^{i-k} (1 - \alpha)^k \quad (3)$$

Solving the convolution equation to retrieve the IRF was equivalent to determining the parameters of the expansion in Eq. 2: the Laguerre parameter ( $\alpha$ ;  $0 < \alpha < 1$ ), the expansion coefficients ( $c_i$ ) and the order of the expansion ( $I$ ). Optimal values of  $\alpha$  and of the coefficients  $c_i$  were determined by least-squares minimization of the weighted sum of residuals:

$$S = \sum_{n=0}^{N-1} w_n [y_c(n) - y_o(n)]^2 \quad (4)$$

where  $y_c(n)$  is the fluorescence response computed from Eq. 1,  $y_o(n)$  is the observed fluorescence response and  $w_n$  is a weighting factor. The whole fluorescence trace (45–90 points) was used in the minimization from the rise of the input laser pulse to  $>5\%$  of its peak amplitude ( $n = 0$ ) to the decay of the output fluorescence response to  $<5\%$  of its peak amplitude ( $n = N - 1$ ). The same number of points was used for all fluorescence responses measured on a given compound.

Proper selection of the weights  $w_n$  is necessary to obtain an accurate estimate of the fluorescence IRF (12). The weight  $w_n$  is proportional to the inverse of the experimental variance  $\sigma_n^2$  for the measurement at time  $n$ , variance that is not known with the present experimental technique. To estimate the dependence of the variance on the magnitude of the fluorescence signal, we considered the experimental variance at each time point for the 10 fluorescence measurements at 390 nm obtained on dry elastin and dry collagen (21). The variance was represented in log–log coordinates as a function of the average of the 10 measurements. The slope of the straight-line fit through the log–log plot averaged 1.7 (range: 1.3–2.1) for the six data sets, suggesting that the measurement variance increased almost in proportion with the square of the fluorescence signal. Thus, weight  $w_n$  was estimated by  $1/y_o(n)^2$  in Eq. 4 and the least-squares minimization was carried out on the quantity

$$S = \sum_{n=0}^{N-1} \left[ \frac{y_c(n) - y_o(n)}{y_o(n)} \right]^2 \quad (5)$$

to yield parameter  $\alpha$  and the expansion coefficients  $c_i$  for a given expansion order  $I$ .

The decrease of the sum of residuals  $S$  with increasing values of the order  $I$  was examined for a set of representative measurements of elastin fluorescence to establish that  $S$  reached a plateau for values of  $I \geq 4$ . Thus, parameter  $I$  was set at 4, which corresponded to using the first five Laguerre functions to expand the fluorescence IRF. All computations were performed with the software package MATLAB (The MathWorks).

**Data analysis.** Time-resolved fluorescence emission spectra were constructed by piling the IRF obtained at different emission wavelengths to build two-dimensional representations of the fluorescence intensity as a function of time and wavelength. The spectra were corrected for the nonuniform spectral response of the measurement system measured with a calibrated irradiance light source (Oriol, 63358) and normalized to a peak intensity of 1.

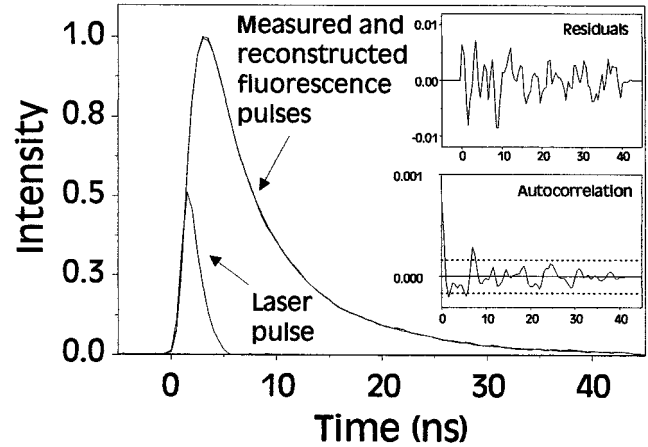


**Figure 2.** Excitation laser pulse and fluorescence emission response. The emission intensity begins to increase at time 0 identified by the rise of the laser trace above its baseline level. The fluorescence response reconstructed by convolution of the laser pulse with the estimated impulse response function overlaps the experimentally measured fluorescence trace. Residuals (top inset) are nearly randomly distributed. Autocorrelation of the residuals (bottom inset) is mostly contained within the 95% confidence interval (dotted lines) centered on the horizontal axis.

Two approaches were used to describe the decay characteristics of the fluorescence IRF at each wavelength. First, a gross measure of the overall decay was estimated from the lifetime ( $\tau$ ) determined as the time at which the IRF crossed the  $1/e$  mark. Second, a finer characterization of the decay was obtained by approximating the IRF with a double-exponential function:

$$h(m) = a_1 e^{-mT/\tau_1} + a_2 e^{-mT/\tau_2} \quad (6)$$

The approximation yielded  $\tau_1$  and  $\tau_2$ , the fast-term and slow-term decay constants, and  $A$ , the ratio  $a_1/(a_1 + a_2)$  that expressed the fractional contribution of the fast decay component to the fluorescence IRF. We selected to approximate the IRF with a double-exponential model after verifying on a representative set of measurements the absence of trends in the residuals (12,22) for the double-exponential model. In addition, the decrease of the weighted residual sum of squares was not significant for a triple-exponential fit when compared with a double-exponential fit (21).

For each compound, parameters  $\tau$ ,  $\tau_1$ ,  $\tau_2$  and  $A$  determined at the wavelengths 390, 430 and 470 nm were analyzed (two-factor analysis of variance) to evaluate the effects of emission wavelength and hydration on these descriptors of the fluorescence decay. When a significant effect was observed, differences among individual means were assessed with a post-hoc Scheffe test. In all analyses, the level of significance was  $P < 0.05$ . Data are reported as mean  $\pm$  SE.

## RESULTS

### Deconvolution method—fluorescence impulse response function

An example of laser pulse and corresponding fluorescence response (type I collagen, 390 nm) is shown in Fig. 2. On the plot, the computed fluorescence response (convolution of laser pulse with fluorescence IRF) is indistinguishable from the observed fluorescence trace. The residuals (top inset) are  $<1\%$  of the peak fluorescence amplitude and they appear randomly distributed around 0. The autocorrelation function of the residuals (bottom inset) is free of low-frequency oscillations characteristic of nonrandom residuals (12,23). Furthermore, it is known that the residuals are not correlated at the 95% confidence level if less than 1 out of 20 autocor-

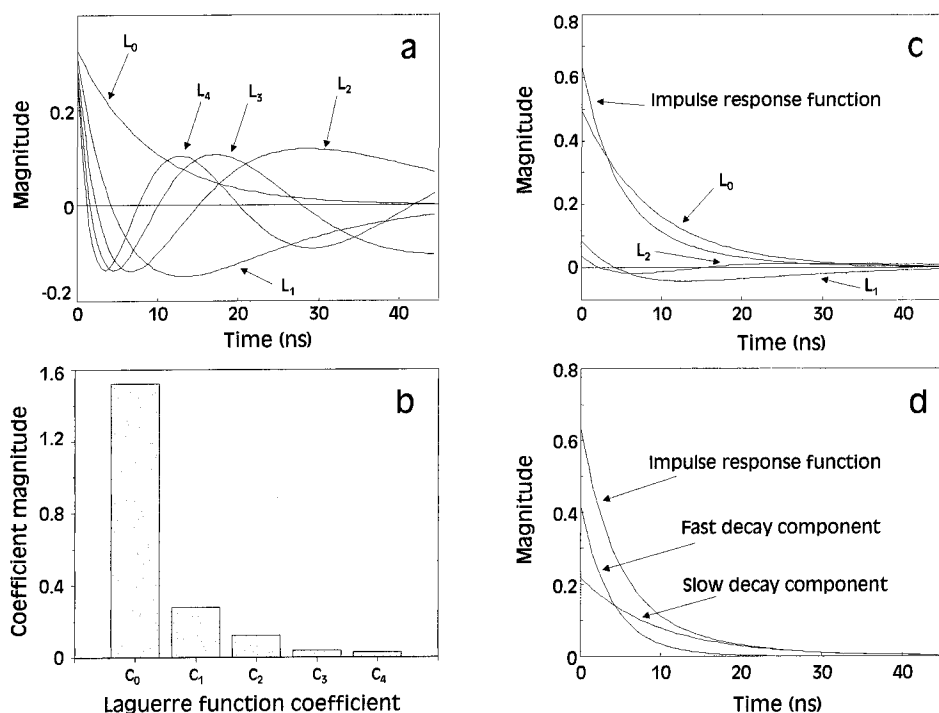


**Figure 3.** Illustration of the deconvolution operation for the experimental data in Fig. 2. a: First five Laguerre functions ( $L_0$ – $L_4$ ) for optimal value of parameter  $\alpha$  (0.85) have characteristic properties discussed in the text. b: Corresponding coefficients ( $c_0$ – $c_4$ ) decrease toward 0 for increasing function order. c: Impulse response function constructed as the weighted sum of functions  $L_0$ – $L_4$  multiplied by the corresponding coefficient  $c_0$ – $c_4$ . Functions  $L_0$ – $L_2$  scaled by the corresponding coefficients are shown. d: Impulse response function approximated as the sum of two (fast and slow) exponential components.

relation values (5%) exceed the symmetric bounds  $\pm 1.96C(0)/\sqrt{N}$  where  $C(0)$  is the autocorrelation for lag 0 and  $N$  is the number of lags (24). In the example of Fig. 2, 5 out of 85 points (6%) exceed the limits expected based on chance, which confirms the near-random distribution of the residuals. The observations indicate excellent fit between the observed and computed fluorescence responses. They are evidence that the fluorescence IRF was properly estimated with the deconvolution algorithm based on the Laguerre expansion technique.

The five Laguerre functions used to estimate the IRF are shown in Fig. 3a. Function  $L_0$  is a decaying exponential with time constant of 6.2 ns (Laguerre parameter  $\alpha = 0.85$ ). The number of crossings of the horizontal axis (zeros of the function) is equal to the function order for the higher order functions ( $L_1$ : one zero;  $L_2$ : two zeros, . . .). Higher order functions decay faster toward their first zero than lower order functions and therefore serve to reproduce the fast dynamics of the IRF. The corresponding coefficients  $c_i$  of the IRF expansion (Fig. 3b) decrease rapidly toward 0 such that the contribution of functions  $L_3$  and  $L_4$  to the IRF reconstruction is much smaller than that of the Laguerre functions of lower order. This observation supports our choice of limiting the expansion of the fluorescence IRF to five Laguerre functions (17). The IRF decays faster toward 0 than the exponential  $L_0$  (Fig. 3c) because functions on the order of  $\geq 1$  rapidly become negative and depress the IRF relative to function  $L_0$ . The average lifetime  $\tau$  is 5.4 ns. The double-exponential approximation of the IRF (Fig. 3d) yields  $\tau_1 = 4.0$  ns,  $\tau_2 = 9.8$  ns and  $A = 0.66$ . These values agree with a duration of 390 nm emission for type I collagen ( $\geq 20$  ns).

#### Time-resolved fluorescence emission spectra

The time-resolved fluorescence spectra of the dry arterial fluorescent compounds (Fig. 4) presented marked differences

in the time dimension, with collagen emission lasting the longest time and cholesterol emission the shortest time. The emission at 390 nm (near the peak of emission for the three compounds) decreased to 5% of its value at time 0 in approximately 11 ns for elastin, 20 ns for type I collagen and 5 ns for cholesterol. For elastin, the temporal profile of the emission lasted slightly longer for higher wavelengths. In contrast, collagen emission decayed faster toward zero when wavelength was increased. For cholesterol, the fluorescence emission at wavelengths between 470 and 490 nm increased after time 0 and was maximum at time 0.5 ns.

In the wavelength dimension, the time-resolved fluorescence spectra were similar in shape to the steady-state emission spectra measured with CW excitation. Numerical integration of the temporal profile at each wavelength yielded reconstructed steady-state spectra (insets) in agreement with previously reported observations (2–4). Elastin had a broad peak with maximum at 410–420 nm and a half width at half maximum (HWHM; measured on the long wavelength side of the peak) of 75 nm. Type I collagen had a narrow peak with a maximum at 385 nm and an HWHM  $< 40$  nm. Cholesterol emission was maximum at 370 nm and its HWHM was similar to that of type I collagen.

#### Variation of average lifetime with wavelength and with hydration

Elastin, type I collagen and cholesterol had significantly different average lifetimes, collagen having the longest  $\tau$  and cholesterol the shortest  $\tau$  (Fig. 5). This was true for both the dry and the hydrated compounds. Elastin lifetime increased slightly but significantly between 390 nm ( $2.3 \pm 0.1$  ns; dry form) and 430 nm. Elastin lifetime at 470 nm was not different from that measured at 390 nm. Hydration did not change the average lifetime of elastin.

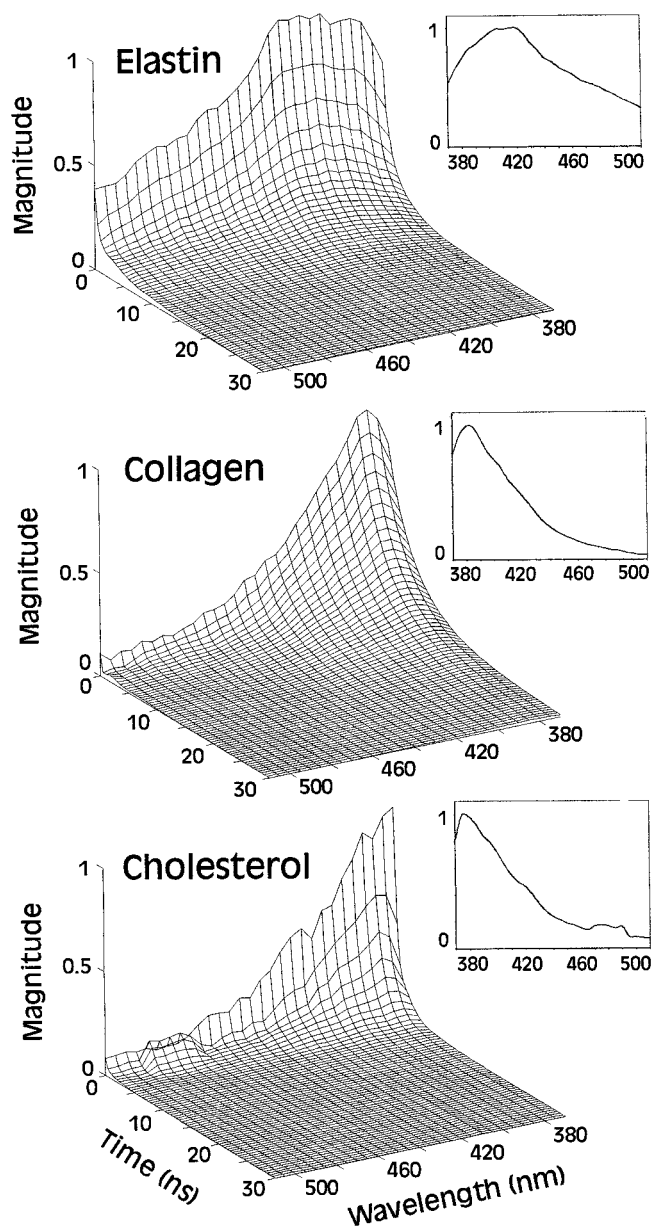


**Figure 4.** Time-resolved fluorescence spectra of elastin (top panel), collagen (middle panel) and cholesterol (bottom panel) in dry form. Magnitude of fluorescence impulse response function varies as a function of time (in ns) and emission wavelength (in nm). Insets show CW spectra reconstructed by integration of the time-resolved decays along the time dimension. Note that in the time-resolved spectra, the wavelength dimension increases from back to front (right to left). Wavelengths increase from left to right in the CW spectra.

For dry collagen, the lifetime was nearly constant for wavelengths  $<430$  nm (390 nm:  $5.3 \pm 0.1$  ns) and it decreased gradually for higher wavelengths. Hydrated collagen had a smaller lifetime than dry collagen for wavelengths  $<430$  nm (390 nm:  $4.3 \pm 0.1$  ns). Collagen lifetime was independent of hydration for wavelengths  $\geq 430$  nm.

The average lifetime of cholesterol was approximately constant (390 nm:  $1.3 \pm 0.1$  ns) for wavelengths  $<470$  nm. For wavelengths between 470 nm and 490 nm, the lifetime was computed from the peak of the IRF at 0.5 ns. In that

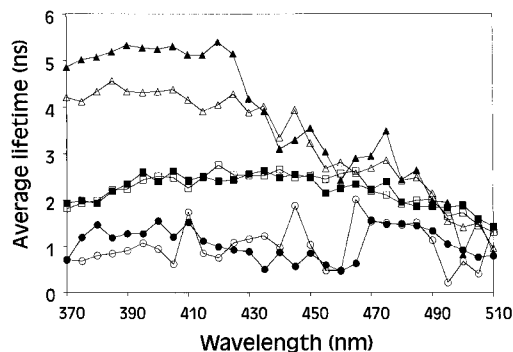


**Figure 5.** Average lifetime as a function of wavelength for elastin ( $\blacksquare$ ,  $\square$ ), collagen ( $\blacktriangle$ ,  $\triangle$ ) and cholesterol ( $\bullet$ ,  $\circ$ ) in dry (filled symbols) and in hydrated form (open symbols). The lifetimes of the three compounds are most different for wavelengths  $<430$  nm. The only effect of hydration is noted for collagen lifetime at wavelengths  $<430$  nm.

range of wavelengths, parameter  $\tau$  ( $1.6 \pm 0.1$  ns) was larger than the values observed at the other wavelengths. Cholesterol lifetime was independent of hydration.

#### Variation of biexponential decay characteristics with wavelength and with hydration

The variations of decay parameters  $\tau_1$ ,  $\tau_2$  and A revealed that the shape of the fluorescence IRF changed with wavelength and with hydration for the three fluorescent compounds (Figs. 6 and 7). For dry elastin (Fig. 6), the fast decay constant  $\tau_1$  (390 nm:  $1.3 \pm 0.1$  ns) was invariant and the slow decay constant  $\tau_2$  (390 nm:  $5.7 \pm 0.1$  ns) gradually increased when wavelength was increased. The fractional contribution of the fast decay term A (390 nm:  $0.63 \pm 0.01$ )

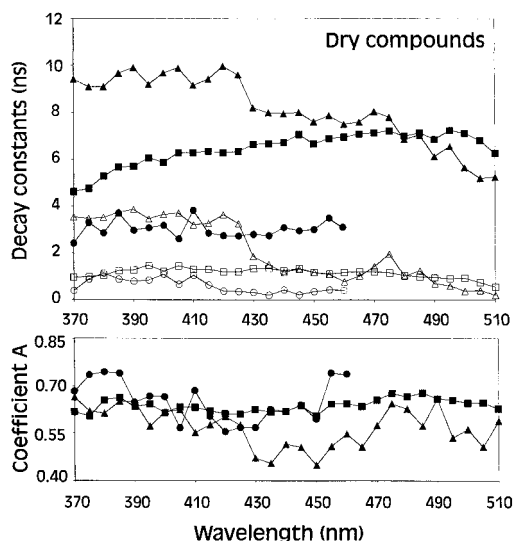


**Figure 6.** Time-resolved fluorescence decay parameters for elastin ( $\blacksquare$ ,  $\square$ ), collagen ( $\blacktriangle$ ,  $\triangle$ ) and cholesterol ( $\bullet$ ,  $\circ$ ) in dry form. Top panel: Fast decay constant  $\tau_1$  (filled symbols) and slow decay constant  $\tau_2$  (open symbols); bottom panel: fractional contribution of fast decay component A. Elastin parameters  $\tau_2$  and A and collagen parameters  $\tau_1$ ,  $\tau_2$  and A changed with wavelength to represent wavelength-dependent variations of the fluorescence impulse response function for the two compounds. Cholesterol decay parameters were unaffected by wavelength.

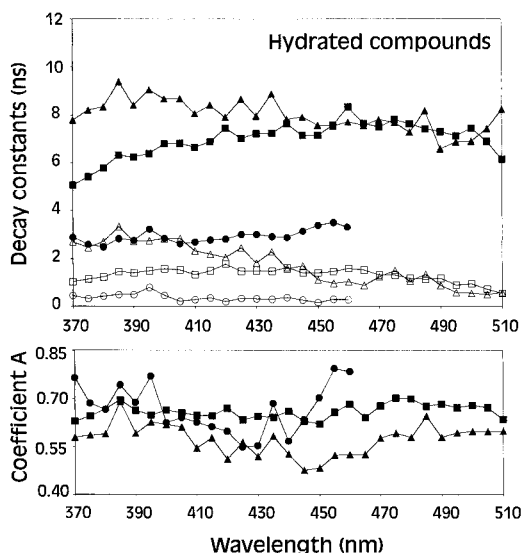


**Figure 7.** Time-resolved fluorescence decay parameters for elastin (■, □), collagen (▲, △) and cholesterol (●, ○) in hydrated form. Top panel: fast decay constant  $\tau_1$  (filled symbols) and slow decay constant  $\tau_2$  (open symbols); bottom panel: fractional contribution of fast decay component A. Variations of elastin decay parameters were similar to those observed on the dry compound. Collagen parameters  $\tau_1$  and A changed as they had for the compound in dry form.

slightly increased with increasing wavelengths. These variations combined to yield an IRF that decreased more steeply shortly after time 0 but that lasted longer in time at the longer wavelengths. On average, the decay descriptors were slightly larger ( $\tau_1$  by 0.1 ns;  $\tau_2$  by 0.5 ns; A by 0.02) for hydrated elastin compared to dry elastin (Fig. 7). The wavelength-related variations of the decay descriptors  $\tau_1$ ,  $\tau_2$  and A were similar for hydrated elastin and for dry elastin.

Decay constants  $\tau_1$  (390 nm:  $3.9 \pm 0.1$  ns) and  $\tau_2$  ( $9.9 \pm 0.2$  ns) measured on dry collagen exhibited a sudden drop at 430 nm and continued to decrease for higher wavelengths (Fig. 6). Parameter A (390 nm:  $0.65 \pm 0.02$ ) decreased toward a minimum at wavelengths between 430 and 450 nm before increasing at higher wavelengths. The combined effect of these variations was a substantially steeper decay of the collagen fluorescence IRF for wavelengths  $\geq 430$  nm compared to the IRF decay observed at lower wavelengths. Hydration resulted in a marked decrease of decay parameters  $\tau_1$  (390 nm:  $2.7 \pm 0.1$  ns),  $\tau_2$  ( $8.4 \pm 0.2$  ns) and A ( $0.59 \pm 0.02$ ) for wavelengths  $< 430$  nm relative to the dry state (Fig. 7). The decay parameters were not affected by hydration for wavelengths  $\geq 430$  nm. The wavelength-related variations of  $\tau_1$  and A observed on hydrated collagen resembled those measured on dry collagen. Decay constant  $\tau_2$  measured on hydrated collagen did not change with wavelength.

Cholesterol decay parameters  $\tau_1$  (390 nm:  $0.8 \pm 0.1$  ns),  $\tau_2$  (390 nm:  $3.0 \pm 0.3$  ns) and A (390 nm:  $0.65 \pm 0.03$ ) did not vary for emission wavelengths between 370 and 460 nm (Fig. 6). These parameters were also not changed by hydration (Fig. 7). Note that the parameters of the biexponential fit were not computed for wavelengths above 460 nm due to the shape of the cholesterol fluorescence IRF for wavelengths between 470 and 490 nm (Fig. 4).

## DISCUSSION

This study investigated the time-resolved fluorescence spectra of elastin, collagen and cholesterol reconstructed with the Laguerre expansion technique to determine the applicability of this new deconvolution technique and to examine variations of the fluorescence decay of these compounds with wavelength and with hydration. The principal findings were as follows. First, the Laguerre expansion technique could successfully reconstruct time-dependent fluorescence decays obtained with nanosecond excitation without imposing a multiexponential structure on the decay profile. Second, the fluorescence emission of the three arterial compounds decayed at markedly different rates that were wavelength dependent such that the largest difference between decay rates was observed for wavelengths below 430 nm. Third, collagen was the only compound whose fluorescence decay was markedly hydration dependent, the effect of hydration being noticed in the blue range of the emission spectrum.

### Deconvolution of fluorescence decay with the Laguerre expansion technique

The proposed deconvolution method for retrieving the fluorescence IRF relies on the well-known LSIR technique (12–15) to compute the parameters of an expansion of the IRF on a discrete-time Laguerre basis. Grinvald and Steinberg (12) were among the first to apply LSIR to deconvolve fluorescence decays measured with excitation pulses of finite duration. These authors expanded the fluorescence IRF on a small set of exponential functions, but they pointed out that LSIR could be used with other types of functional expansion. Since that early study, detailed comparisons of different deconvolution methods have been conducted on simulated data and on fluorescence responses of compounds with known emission decay (14,15). The studies concluded that LSIR was the most reliable method to retrieve the decay constants for complicated systems and in the presence of experimental artifacts.

When the compound under investigation is poorly characterized, the parameters of a multiexponential fit of the fluorescence IRF cannot readily be interpreted in terms of fluorophore content (13). Very different multiexponential expressions can reproduce experimental fluorescence decay data equally well in the presence of measurement noise (24,25). Ware *et al.* (16) introduced the exponential series method that expresses the IRF as the sum of a large number of exponential functions with fixed decay constants. These authors insisted on the fact that for complex fluorescent systems, there was an advantage in avoiding any assumption about the functional form of the decay law during the deconvolution. They suggested that the IRF expressed as an exponential series could be investigated after the deconvolution was completed to test different models of the underlying photoprocesses.

The Laguerre expansion technique is similar to the exponential series method in that it yields a model-free representation of the fluorescence IRF (17,20). Its main benefit is that for any value of the Laguerre parameter  $\alpha$ , the corresponding basis of Laguerre functions is a complete family for the space of square integrable functions. Thus, it is certain that a weighted sum of Laguerre functions can be found

to represent a fluorescence IRF of any form. In contrast, deconvolution with the exponential series method is successful only when the decay constants fixed *a priori* are commensurate with the fluorescence decay under investigation (16). Marmarelis (17) popularized the Laguerre expansion technique for analysis of dynamic linear and nonlinear systems. He demonstrated that it was an effective technique to estimate the intrinsic properties of a system—the IRF for a linear system—from short input–output data records. The asymptotic exponential decline of Laguerre functions was well suited to describe the IRF of physical systems that commonly die out as decaying exponentials. Marmarelis (17) proposed to use a least-squares optimization procedure analogous to LSIR to determine the coefficients of the Laguerre expansion. In principle, the Laguerre parameter  $\alpha$  could be fixed *a priori* to any value between 0 and 1. A value of  $\alpha$  that matched the decay characteristics of the IRF led to a smaller number of Laguerre functions in the expansion (17). In the present study, the selection of parameter  $\alpha$  was automated as a part of the least-squares minimization. The Laguerre expansion technique was found to be well suited for deconvolving the fluorescence decay of arterial compounds.

Application of the Laguerre expansion technique amounts to dissociating the computation of the IRF from the analysis of the fluorescence decay in terms of time-dependent processes. It has been pointed out (16,24) that there were advantages to separating the two steps. This observation is especially important for time-resolved fluorescence measurements in biological tissues. In such systems, the fluorophores are often not well characterized in the tissue environment. The fluorophore distribution in the volume probed by the measurement is not known. Furthermore, the propagation of light at the wavelengths of excitation and emission determines the size of the interrogated volume and therefore the experimental fluorescence spectrum (26). Use of the Laguerre expansion technique for deconvolution of fluorescence decay measurements should simplify the application of time-resolved fluorescence spectroscopy for nondestructive analysis of biological tissues.

In this study, we did not compare the performance of the Laguerre expansion technique to that of a multiexponential expansion of the IRF. Our primary goal was to investigate the applicability the Laguerre expansion technique, which we found yielded an accurate estimation of the measured fluorescence curves based on the magnitude and randomness of the residuals and autocorrelation of residuals (12,22). The comparative analysis would have been of limited interest because the decay characteristics of the fluorescent compounds of the arterial wall are not well known. Comparison of the decay trends afforded by the two functional expansions with standard values would not have been possible.

*Time-resolved fluorescence of arterial fluorescent compounds.* Studies on the CW fluorescence of dissolved elastin and collagen (27–30) identified the principal fluorophores that contribute to the emission of these compounds. The information can be used to interpret the decay trends identified by biexponential approximation of the IRF (13). Chromatographic analysis of acid-hydrolyzed bovine elastin resolved two dominant fluorophores with spectral peaks at 304/394 nm (excitation/emission) and 336/398 nm and three minor fluorophores with peaks at 330/422, 352/432 and 362/440

nm (27,28). It is likely that with excitation at 337 nm, the emission spectrum we measured for elastin was dominated by the 336/398 nm fluorophore with lesser contributions from the other fluorophores. The shift of the emission peak to 410 nm in our measurements was probably due to the emission of the minor fluorophores and possibly also to the fact that elastin was studied in nondissolved form as opposed to dissolved in hydrochloric acid. The minor fluorophores have emission peaks above 420 nm and their contribution to the elastin spectrum is likely to increase on the red side of the spectrum. We observed that the slow decay constant  $\tau_2$  increased with increasing wavelength, which suggests longer lifetimes for the minor fluorophores compared to the lifetime of the dominant fluorophore.

Fujimoto (29) attributed the dominant fluorescence peak (325/410 nm) of bovine Achilles tendon collagen to the amino-acid crosslink pyridinoline. In a subsequent study (30), Fujimori identified two main emission peaks for solubilized Achilles tendon collagen. The first peak (325/390 nm) originated from pyridinoline crosslinks while the second spectral feature was three-peaked (300/350, 300/370 and 300/385 nm) and mostly caused by the emission of collagen monomers and small chains. Based on these studies, the time-resolved spectrum of collagen in our study must have predominantly originated from the emission of pyridinoline with a likely contribution of the monomeric chains on the blue side of the spectrum. The average lifetime and the time decay constants of collagen decreased sharply at 430 nm, suggesting that the 350–385 nm fluorophores ceased to fluoresce above that wavelength.

While there is abundant information on the CW fluorescence spectra of elastin and collagen, much less has been reported on their time-resolved emission characteristics. Andersson-Engels *et al.* (8–10) measured the time-resolved fluorescence of these materials at selected wavelengths using picosecond excitation at 337 nm. They found, as we have, that elastin emission decayed much faster than collagen emission. The authors (10) used three exponentials to approximate the fluorescence decay at 380 nm (elastin:  $\tau_1 = 2.1$  ns,  $\tau_2 = 6.6$  ns,  $\tau_3 = 0.4$  ns; collagen:  $\tau_1 = 5.0$  ns,  $\tau_2 = 9.9$  ns,  $\tau_3 = 0.8$  ns) and two exponentials to approximate the emission decay of elastin at 520 nm ( $\tau_1 = 1.4$  ns,  $\tau_2 = 6.7$  ns). We found that two exponential components could approximate the fluorescence decay of compounds across the emission spectrum. In previous work (20), we showed that decay constants down to 1 ns could be retrieved with accuracy with our experimental setup and deconvolution method. Subnanosecond decays could also be retrieved, albeit with an overestimation of the decay constants. Given the values of the fast decay constant  $\tau_1$  for elastin and collagen (elastin:  $\tau_1 = 1.3$  ns; collagen:  $\tau_1 = 3.9$  ns at 390 nm), we surmise that the decay characteristics of the compounds were properly estimated. It is possible that the two faster exponential components measured by Andersson-Engels *et al.* at 380 nm became lumped into a single decay trend in our computations. The exponential approximation was carried out on the fluorescence IRF expanded on the Laguerre basis in the present study. Because the Laguerre functions of high order render the faster dynamics of the expanded function, using only the first five Laguerre functions for the approximation could have partially filtered out the fastest trends of

the decay. Differences in levels of irradiation (46 mJ/mm<sup>2</sup> in the studies of Andersson-Engels *et al.* versus 1.2 mJ/mm<sup>2</sup> in our experiments) could also have contributed to differences in the fluorescence decays (6). Note that the elastin decay constants estimated by Andersson-Engels *et al.* at 520 nm (10) were similar to the average decay rates for wavelengths >450 nm in our study ( $\tau_1 = 1.1$  ns,  $\tau_2 = 7.0$  ns).

The fluorescence of cholesterol has been less studied than that of the other arterial compounds and is somewhat controversial (31). Structural features in cholesterol and other steroid molecules absorb UV energy (32) and could be responsible for the fluorescence emission. Laifer *et al.* (2) and Yan *et al.* (4) observed measurable fluorescence emission for purified cholesterol excited at 325 and 308 nm, respectively. The CW spectra were maximum around 375 nm and the emission intensity decreased sharply as wavelength increased. The CW fluorescence spectrum of cholesterol obtained by time integration in the present work was similar to the data presented by these two groups. The fluorescence of lipid extract from human atherosclerotic aorta resembled the emission measured on cholesterol (2). Cholesterol content correlated with features of the fluorescence spectra measured on atherosclerotic rooster aorta (4). These observations suggest that cholesterol contributes to the fluorescence emission of lipid-rich atherosclerotic plaque. Two time constants independent of wavelength were identified in the time-resolved spectrum of cholesterol below 460 nm. This result is consistent with the existence of two distinct fluorophores in cholesterol. The slow decay constant  $\tau_2$  (~3.0 ns) was well within the range of capability of our instrumentation and deconvolution method. In contrast, the fast decay component  $\tau_1$  (0.5–0.8 ns) was probably overestimated.

For wavelengths between 470 and 490 nm, the intensity of cholesterol emission increased between 0 and 0.5 ns. A buildup of fluorescence intensity prior to the decay has been linked to the formation of fluorescent excited species in different types of biological molecules (25,33). The red shift relative to the emission of the primary fluorophore results from utilization of energy in the excited-state reactions (25). The nature of the excited-state process cannot be described in detail using the present results. However, we note that similar time shifts of the fluorescence peak at 470–490 nm have been reported for two cholesterol esters present in atherosclerotic lesions (11) and in the time-resolved spectra of lipid-rich atherosclerotic samples of human aorta (34). This spectral feature could serve to recognize the presence of cholesterol and associated lipids in arterial lesions (11).

#### Effect of hydration on arterial compound fluorescence

The time-resolved fluorescence spectra of elastin and cholesterol were minimally affected by hydration. For both compounds, the average lifetime was independent of hydration at all emission wavelengths. The shape of the elastin decay profile changed slightly with hydration; that of cholesterol was not altered. These observations suggest that the fluorophores in the two compounds do not interact with water molecules in the microenvironment. Collagen time-resolved fluorescence was also unaffected by hydration for wavelengths above 430 nm. In contrast, hydration markedly shortened the lifetime and decay constants of collagen fluores-

cence for wavelengths below 430 nm. Comparison of the CW spectra of collagen in dry and in hydrated form showed that hydration reduced the emission intensity in the blue range relative to the red range of the spectrum. Hydration has been shown to alter the fluorescence lifetime of different proteins (18,19), possibly because of a loosening of the molecular structure, which allows for some fluorophore to sample quenching environments during the excited-state lifetime (19). We suggested that collagen monomers and small chains contribute to the emission spectrum below 430 nm. Hydration could increase the flexibility of the collagen structure and result in quenching of the monomeric chain fluorescence. Decreased fluorescence of the monomers associated with hydration would explain both the decrease in the emission intensity and the changed lifetime in the blue range of the collagen spectrum.

#### Application to optical analysis of the arterial wall

The idea of using time-resolved fluorescence spectroscopy to identify atherosclerotic lesions is not new. A few studies (7–9) measured the time-resolved emission of tissue samples at a few wavelengths and observed that the fluorescence decay of healthy arterial wall was shorter than that of atherosclerotic plaque. The difference was attributed to the shorter lifetime of elastin compared to that of collagen (10). The present results confirmed the latter observation. Because we measured the time-resolved decay at many wavelengths, we were able to show that the choice of the detection wavelength conditioned the ability to discriminate between arterial fluorescent compounds based on their time-resolved emission profile. The time-resolved decays were most different for emission wavelengths below 420 nm. The difference between decay rates tapered off as the emission wavelength was raised above that bound. Several studies have shown that differences in the CW fluorescence spectra of healthy and atherosclerotic arterial tissue paralleled the spectral differences that exist between the CW emission of elastin and that of collagen (2–4). It is reasonable to assume that the differences in the time-dependent characteristics of elastin and collagen identified in the present study would similarly translate in emission decay differences between healthy and atherosclerotic tissue. Indeed, the time-dependent emission of atherosclerotic aortic samples lasted longer than that of healthy aortic wall below 430 nm but not above that wavelength (34). Therefore, the present results suggest that one should preferentially target the blue range of the emission spectrum when designing a nondestructive optical biopsy system for atherosclerosis detection based on time-resolved fluorescence spectroscopy.

Discrimination between graded levels of atherosclerosis has been demonstrated using graded features of the CW fluorescence emission of healthy and diseased aortic wall (5). The accuracy of the discrimination should increase if one capitalized on differences in the time dimension of the spectra in addition to differences in the spectral dimension. We have found that the time-dependent decay profile changed as a function of the emission wavelength for both elastin and collagen. Classification of artery samples between types of atherosclerotic lesions with different elastin and collagen content should be enhanced by measuring the fluorescence

time-dependent profile at multiple wavelengths. A few wavelengths should suffice because the changes in the time-dependent decay were gradual for the arterial fluorescent compounds examined in the present study. In addition, our results suggest that optical detection of free cholesterol in lipid-rich atherosclerotic lesions may be possible. Cholesterol would be recognized from other fluorescent substances by its fast fluorescence decay rate and its delayed emission at 470–490 nm. As noted in a preceding paragraph, similar characteristics have been observed in the time-resolved emission spectra of cholesterol and of lipid-rich aortic lesions for wavelengths between 470 and 490 nm (34). These features could serve to improve the discrimination between lipid-rich atherosclerotic lesions and more advanced collagen-rich fibrous lesions.

Finally, we showed that hydration affected the fluorescence decay rate of collagen and reduced the difference in lifetime between elastin and collagen. The fluorescence lifetime of collagen in the watery environment of the atherosclerotic arterial wall can be expected to be smaller than the lifetime of dry collagen. Other factors in the tissue environment such as temperature and pH could modify the temporal emission profile of arterial fluorescent compounds. The effects of environmental factors on the time-resolved fluorescence spectra of purified compounds will need to be examined experimentally before one can reliably interpret the spectra measured on artery tissue in terms of composition. Such studies would help ascertain the usefulness of time-resolved fluorescence spectroscopy for nondestructive optical biopsy of the arterial wall.

## Conclusion

This study established the feasibility of using the Laguerre expansion technique to deconvolve the time-resolved emission of arterial fluorescent compounds excited with nanosecond laser pulses. Deconvolution with the Laguerre expansion technique separated the computation of the fluorescence IRF from the modeling of the fluorescent system. This feature could facilitate the interpretation of time-resolved fluorescence measurements performed in biological media. Substantial differences in the time-resolved fluorescence spectra of the main arterial fluorescent compounds were identified that could serve as diagnostic markers for optical analysis of the arterial wall.

**Acknowledgements**—This work was supported in part by the American Heart Association, Greater Los Angeles Affiliate (#1082-GI), the Charles Lee Powell Foundation, the Biomedical Simulation Resource at the University of Southern California and the Medallions Group, Cedars Sinai Medical Center. The authors are grateful to Dr. Vasilis Marmarelis for helpful discussions and to Mr. Thanassis Papaioannou for his technical assistance.

## REFERENCES

- Kittrell, C., R. L. Willett, S. de los Santos-Pacheo, N. B. Ratiff, J. R. Kramer, E. G. Malk and M. S. Feld (1985) Diagnostic of fibrous arterial atherosclerosis using fluorescence. *Appl. Opt.* **24**, 2280–2281.
- Laifer, L. I., K. M. O'Brien, M. L. Stetz, G. R. Gindi, T. J. Garrand and L. I. Deckelbaum (1989) Biochemical basis for the difference between normal and atherosclerotic arterial fluorescence. *Circulation* **80**, 1893–1901.
- Baraga, J. J., R. P. Rava, P. Taroni, C. Kittrell, M. Fitzmaurice and M. S. Feld (1990) Laser induced fluorescence spectroscopy of normal and atherosclerotic human aorta using 306–310 nm excitation. *Lasers Surg. Med.* **10**, 245–261.
- Yan, W. D., M. Perk, A. Chapgar, Y. Wen, S. Stratoff, W. J. Schneider, B. I. Jugdutt, J. Tulip and A. Lucas (1995) Laser-induced fluorescence: III. Quantitative analysis of atherosclerotic plaque content. *Lasers Surg. Med.* **16**, 164–178.
- Morguet, A. J., R. E. Gabriel, A. B. Buchwald, G. S. Werner, R. Nyga and H. Kreuzer (1997) Single-laser approach for fluorescence guidance of excimer laser angioplasty at 308 nm: evaluation in vitro and during coronary angioplasty. *Lasers Surg. Med.* **20**, 382–393.
- Marcu, L., W. S. Grundfest and J. M. Maarek (1999) Photobleaching of arterial fluorescent compounds: characterization of elastin, collagen, and cholesterol time-resolved spectra during prolonged ultraviolet irradiation. *Photochem. Photobiol.* **69**, 713–721.
- Baraga, J. J., P. Taroni, Y. D. Park, K. An, A. Maestri, L. L. Tong, R. P. Rava, C. Kittrell, R. R. Dasari and M. S. Feld (1989) Ultraviolet laser induced fluorescence of human aorta. *Spectrochim. Acta* **45A**, 95–99.
- Andersson-Engels, S., J. Johansson and S. Svanberg (1990) The use of time-resolved fluorescence for diagnosis of atherosclerotic plaque and malignant tumours. *Spectrochim. Acta* **46A**, 1203–1210.
- Andersson-Engels, S., J. Johansson, K. Svanberg and S. Svanberg (1991) Fluorescence imaging and point measurements of tissue: applications to the demarcation of malignant tumors and atherosclerotic lesions from normal tissue. *Photochem. Photobiol.* **53**, 807–814.
- Andersson-Engels, S., L. Baert, R. Berg, M. A. D'Hallewin, J. Johansson, U. Stenram, K. Svanberg and S. Svanberg (1991) Fluorescence characteristics of atherosclerotic plaque and malignant tumors. *SPIE Proc.* **1426**, 31–43.
- Marcu, L., J. M. Maarek and W. S. Grundfest (1998) Time-resolved laser induced fluorescence of lipids involved in development of atherosclerotic lesion lipid-rich core. *SPIE Proc.* **3250**, 158–167.
- Grinvald, A. and I. Z. Steinberg (1974) On the analysis of fluorescence decay kinetics by the method of least squares. *Anal. Biochem.* **59**, 583–598.
- Lakowicz, J. R. (1983) *Principles of Fluorescence Spectroscopy*, pp. 51–91. Plenum Press, New York.
- McKinnon, A. E., A. G. Szabo and D. R. Miller (1977) The deconvolution of photoluminescence data. *J. Phys. Chem.* **81**, 1564–1570.
- O'Connor, D. V., W. R. Ware and J. C. Andre (1979) Deconvolution of fluorescence decay curves. A critical comparison of techniques. *J. Phys. Chem.* **83**, 1333–1343.
- Ware, W. R., L. J. Doemeny and T. L. Nemzek (1973) Deconvolution of fluorescence and phosphorescence decay curves. A least-squares method. *J. Phys. Chem.* **77**, 2038–2048.
- Marmarelis, V. Z. (1993) Identification of nonlinear biological systems using Laguerre expansions of kernels. *Ann. Biomed. Eng.* **21**, 573–589.
- Sheats, G. F. and L. S. Forster (1983) Fluorescence lifetimes in hydrated bovine serum albumin powders. *Biochem. Biophys. Res. Commun.* **114**, 901–906.
- Fucaloro, A. F. and L. S. Forster (1985) Conformational fluctuations in  $\alpha$ -chymotrypsinogen A powders. *Photochem. Photobiol.* **41**, 91–93.
- Snyder, W. J., J. M. Maarek, T. Papaioannou, V. Z. Marmarelis and W. S. Grundfest (1996) Biologic fluorescence decay characteristics: determination by Laguerre expansion technique. *SPIE Proc.* **2679**, 150–161.
- Landaw, E. M. and J. J. DiStefano III (1984) Multiexponential, multicompartmental, and noncompartmental modeling. II. Data analysis and statistical consideration. *Am. J. Physiol.* **246**, R665–R677.
- Badea, M. G. and L. Brand (1979) Time-resolved fluorescence measurements. *Methods Enzymol.* **61**, 378–425.
- Jenkins, G. M. and D. G. Watts (1968) *Spectral Analysis and its Applications*, pp. 183–189. Holden-Day, San Francisco.
- James, D. R. and W. R. Ware (1986) Recovery of underlying

- distribution of lifetimes from fluorescence decay data. *Chem. Phys. Lett.* **126**, 7–11.
25. Beechem, J. M. and L. Brand (1986) Global analysis of fluorescence decay: application to some unusual experimental and theoretical studies. *Photochem. Photobiol.* **44**, 323–329.
  26. Richards-Kortum, R., R. P. Rava, R. Cothren, A. Metha, M. Fitzmaurice, N. B. Ratliff, J. R. Kramer and M. S. Feld (1989) A model for extracting of diagnostic information from laser induced fluorescence spectra of human artery wall. *Spectrochim. Acta* **45A**, 87–93.
  27. Tinker, D. H. and A. L. Tappel (1982) Separation of the fluorescent compounds of bovine ligamentum nuchae elastin using sephadex G-10, cellulose phosphate and thin-layer chromatography. *J. Chromatogr.* **249**, 347–358.
  28. Tinker, D. H. and A. L. Tappel (1983) A partial characterization of the major fluorophore of bovine ligamentum. *Connect. Tiss. Res.* **11**, 309–319.
  29. Fujimoto, D. (1977) Isolation and characterization of a fluorescent material in bovine Achilles tendon collagen. *Biochem. Biophys. Res. Commun.* **76**, 1124–1128.
  30. Fujimori, E. (1985) Changes induced by ozone and ultraviolet light in type I collagen: bovine Achilles tendon collagen versus rat tail tendon collagen. *Eur. J. Biochem.* **152**, 299–306.
  31. Smutzer, G., B. F. Crawford and P. L. Yeagle (1986) Physical properties of the fluorescent sterol probe dehydroergosterol. *Biochim. Biophys. Acta* **862**, 361–371.
  32. Acuña-Johnson, P. and A. C. Oehlschlager (1989) Identification of sterols and biologically significant steroids by ultraviolet and infrared spectroscopy. In *Analysis of Sterols and Other Biologically Significant Steroids* (Edited by W. D. Nes and E. J. Parish), pp. 267–84. Academic Press, San Diego.
  33. Grinvald, A. and I. Z. Steinberg (1974) Fast relaxation processes in a protein revealed by the decay kinetics of tryptophan fluorescence. *Biochemistry* **13**, 5170–5178.
  34. Maarek, J. M., L. Marcu and W. S. Grundfest (1998) Characterization of atherosclerotic lesions with laser-induced time resolved fluorescence spectroscopy. *SPIE Proc.* **3250**, 181–189.